Letter

Nonlocal signatures of hybridization between quantum dot and Andreev bound states

Andreas Pöschl,[1] Alisa Danilenko,[1] Deividas Sabonis,[1,2] Kaur Kristjuhan,[1] Tyler Lindemann,[3] Candice Thomas,[3] Michael J. Manfra,[3,4] and Charles M. Marcus[1,*]

[1]*Center for Quantum Devices, Niels Bohr Institute, University of Copenhagen, 2100 Copenhagen, Denmark*
[2]*Laboratory for Solid State Physics, ETH Zürich, CH-8093 Zürich, Switzerland*
[3]*Department of Physics and Astronomy, and Birck Nanotechnology Center, Purdue University, West Lafayette, Indiana 47907, USA*
[4]*School of Materials Engineering, and School of Electrical and Computer Engineering, Purdue University, West Lafayette, Indiana 47907, USA*

(Received 10 January 2022; revised 5 September 2022; accepted 13 September 2022; published 3 October 2022)

We investigate local and nonlocal signatures of hybridization between a quantum dot (QD) state and an extended Andreev bound state (ABS) in a gate-defined InAs nanowire (NW) with multiple side probes. When a QD in one of the side probes was hybridized with an ABS in the NW, a characteristic spectroscopic pattern was observed both locally, i.e., in the probe with the QD, and nonlocally, in the tunnel conductance of a remote probe. Nonlocal signatures of hybridization reveal the extended nature of the ABS.

DOI: 10.1103/PhysRevB.106.L161301

Progress in material growth has enabled the realization of hybrid materials with distinct low-temperature phases [1–4] not observed in the constituent bulk materials [5–11]. An important example is a superconductor grown epitaxially on a semiconductor having gateable carrier density, large negative g-factor, and strong spin-orbit coupling [12–14]. A promising material platform that allows for scalable fabrication of advanced devices in this context are InAs two-dimensional electron gases (2DEGs) proximitized by superconducting Al [15–21]. Devices of suitable geometries allow exploration of various bound states in nanowires (NWs), including Yu-Shiba-Rusinov states, Andreev bound states (ABSs), and Majorana bound states [18,20,22–27].

The use of semiconductor-superconductor hybrids facilitates the realization of electrostatically controlled quantum dots (QDs) coupled to superconductors. This was an enabling factor for experiments demonstrating Cooper pair splitting [28,29]. QDs coupled to ABSs have received considerable attention from theoretical studies, including the use of the QD as a tool for measuring bound state lifetimes [30] or providing Majorana parity readout [21,31–35]. Tunnel coupling can lead to energy level hybridization between a QD and a bound state. This can result in a shift of the bound state energy and an avoided crossing between the subgap resonances stemming from the QD and the ABSs. ABSs at finite energy are pushed toward zero energy when resonantly coupled to the QD. This leads to a characteristic bowtie shape in the form of a zero-crossing of the subgap state. For ABSs at zero energy, the bound states acquire finite energy when brought on resonance with the QD, leading to a diamond-shaped splitting in energy. The observed pattern of subgap states near the resonance condition depends on the nonlocality and the spin structure of bound states and details of the QD [36–41].

In this letter, we perform tunneling spectroscopy of a NW in a geometry that allows measurements at several side branches along the NW length using electrostatic gates patterned on an InAs/Al hybrid heterostructure. A similar configuration has been investigated theoretically [42], and a related experiment has been carried out in a conventional NW with a deposited superconductor and normal metallic side contacts [43]. In addition to ABSs due to bound states in the NW, we find conductance resonances due to accidental QDs in the tunnel barriers. We investigate hybridization of QD states with ABSs in the NW, observing signatures of hybridization both locally, that is, at the position of the accidental QD, and nonlocally, measured on another side probe away from the QD.

Figure 1(a) shows a micrograph of device 1, based on an InAs 2DEG with 5 nm of epitaxial Al. The device consists of an Al strip of width 100 nm and length 5 μm, connected at both ends to large planes of Al that were electrically grounded. Gates labeled W_{kl} were Ti/Au on top of 30 nm HfO_2, as shown in Fig. 1(e). Gates were used to deplete the semiconductor on either side of the Al wire, creating by depletion a quasi-one-dimensional InAs NW self-aligned to the proximitizing Al.

Neighboring gates W_{kl} form a constriction that acts as a tunnel probe. The lead of the probe, away from the tunneling region, is made using the same unetched epitaxial Al. Tunneling across the bare semiconductor region between the Al NW and the Al lead is controlled by a probe gate P_j, as shown in Fig. 1(f). Details of the materials and fabrication are given in the Supplemental Material [44].

The measurement setup is shown schematically in Fig. 1(a). With the NW grounded, individual voltage biases $V_{SD}^{(j)}$ were applied on probe j via current-to-voltage converters ($j \in \{1, 2, 3\}$). Tunneling currents I_j through the tunnel barriers were measured using lock-in detection, yielding differential conductances $G_j = dI_j/dV_{SD}^{(j)}$. Measurements were

*marcus@nbi.dk

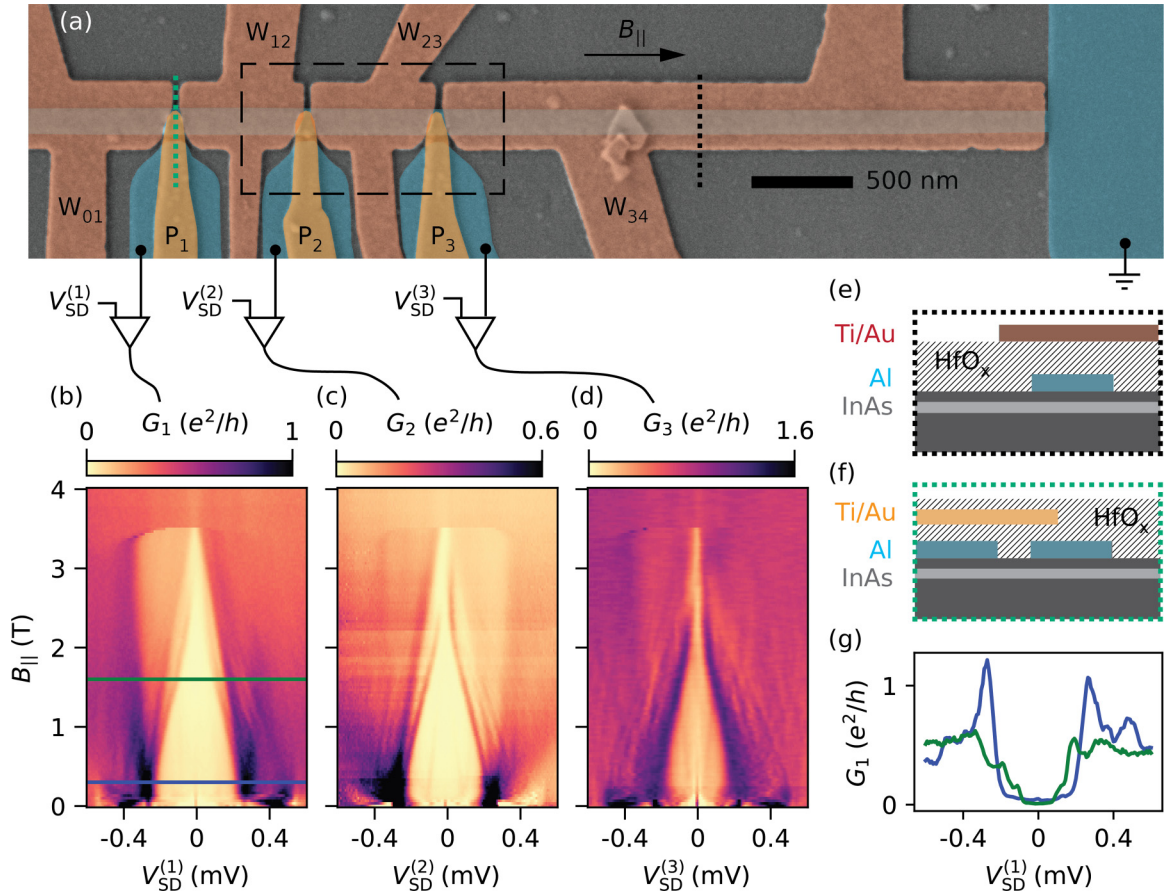

FIG. 1. (a) False-colored scanning electron micrograph of device 1. The device consists of patterned epitaxial Al, forming a long, narrow nanowire with several tunnel probes on top of an InAs quantum well. Gates labeled P_j are used to tune the tunnel barrier between the tunnel probe j and the wire ($j \in \{1, 2, 3\}$). Gates labeled W_{kl}, with $kl \in \{01, 12, 23, 34\}$, deplete carriers except under the Al. (b)–(d) Tunneling spectroscopy at three probes with all gate voltages $V_{Wkl} = -4.5$ V. (e) and (f) Schematic cross-sections of the device at the positions given by the green and black dotted lines in (a). (g) Line cuts at field values $B_{||} = 0.3$ and 1.6 T indicated by the blue and green line in (b).

carried out in a cryo-free dilution refrigerator with a 6-1-1 T vector magnet at ≈15 mK mixing-chamber temperature.

Tunneling conductances G_j as a function of magnetic field $B_{||}$ applied parallel to the NW are shown in Figs. 1(b)–1(d). For weak tunneling and in the absence of probe resonances, G_j is proportional to the density of states in the NW. The superconducting gap of the Al in the leads of the probes closes at low field $B_{||} \approx 0.2$ T, above which the probes can be regarded as normal metal, as discussed previously [16,20]. The semiconductor under the Al in the NW was depleted by setting all W_{kl} gates to −4.5 V. Measurements on all three probes showed a superconducting gap closing without any subgap states crossing zero energy. For G_1, this is illustrated by the line cuts in Fig. 1(g). A splitting of the continuum of states at high bias due to the Zeeman effect can be seen in G_1 and G_2. Note that the measurement of G_3 shows finite subgap conductance, which we attribute to probe 3 being tuned to an open regime with high-bias conductance $G_3(V_{SD}^{(3)} = 0.4\,\text{mV}) \gtrsim 1\ e^2/h$.

To investigate the hybridization of a probe QD state with an ABS in the NW, we focus on the 0.6 µm long NW segment under gate W_{23}, see dashed box in Fig. 1(a), shown in Fig. 2(a). To create an ABS in this segment, the voltage on gate W_{23} was set less negative, in the range of −3 V, while voltages on neighboring gates W_{12} and W_{34} were set to −7.0 V. At $B_{||} = 1.6$ T and zero source-drain biases, $V_{SD}^{(j)} = 0$, conductances G_2 and G_3 were measured as functions of probe-gate voltages V_{P2} and V_{P3}, respectively, and wire-gate voltage V_{W23}. For both tunnel junctions, two sets of conductance resonances can be distinguished in Figs. 2(b) and 2(c) by their characteristic slope. The first set primarily consists of vertical features that are strongly dependent on the gate voltages V_{P2} (V_{P3}), which we attribute to QDs in the tunnel barriers. The second set are predominantly horizontal, depending more strongly on V_{W23}. The latter resonances are visible in both G_2 and G_3, suggesting that they arise from ABSs that extend over the segment covered by gate W_{23}. Figure S1 in the Supplemental Material [44] shows the complete evolution of tunneling spectroscopy from $V_{W23} = -3.8$ to −3.0 V while keeping the tunnel barriers at roughly constant transparency. This was achieved by compensating the effect of the gate W_{23} on the tunnel barriers by changing the gate voltages V_{P2}, V_{P3} given by the green dashed line in Figs. 2(b) and 2(c).

The blue star markers in Figs. 2(b) and 2(c) at gate voltages $V_{W23} = -3.09$ V, $V_{P2} = -0.045$ V, and $V_{P3} = -0.170$ V mark ABSs that are weakly tunnel coupled to the probes. Tunneling spectroscopy of these ABSs as a function of magnetic field $B_{||}$ in Figs. 3(a) and 3(b) reveals a zero-bias crossing of

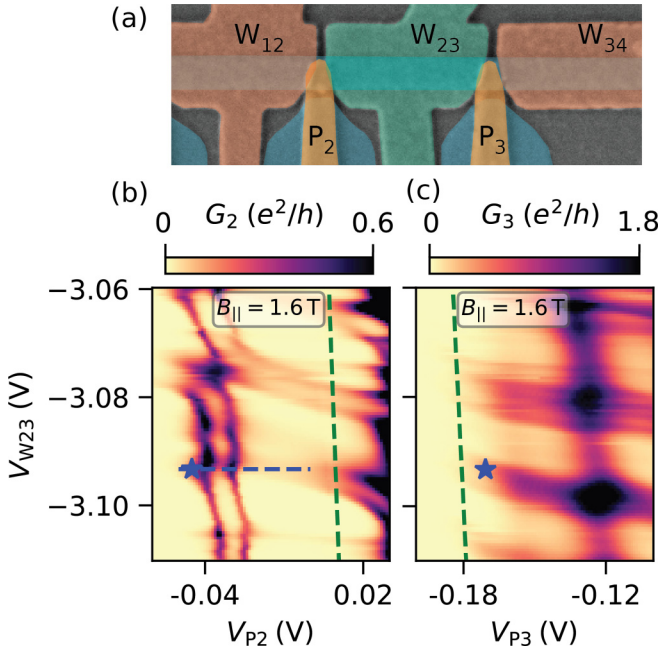

FIG. 2. (a) Micrograph of the nanowire (NW) segment under investigation. $V_{W12} = V_{W34} = -7.0\,\mathrm{V}$ while the voltage on gate W_{23} (green) is varied. (b) and (c) Differential conductance at zero bias measured at the left and the right end of the NW segment. Horizontal conductance resonances appear in both maps at similar gate voltages. Vertical conductance features, strongly dependent on gates V_{P2} and V_{P3} which tune the tunnel barriers, are also visible.

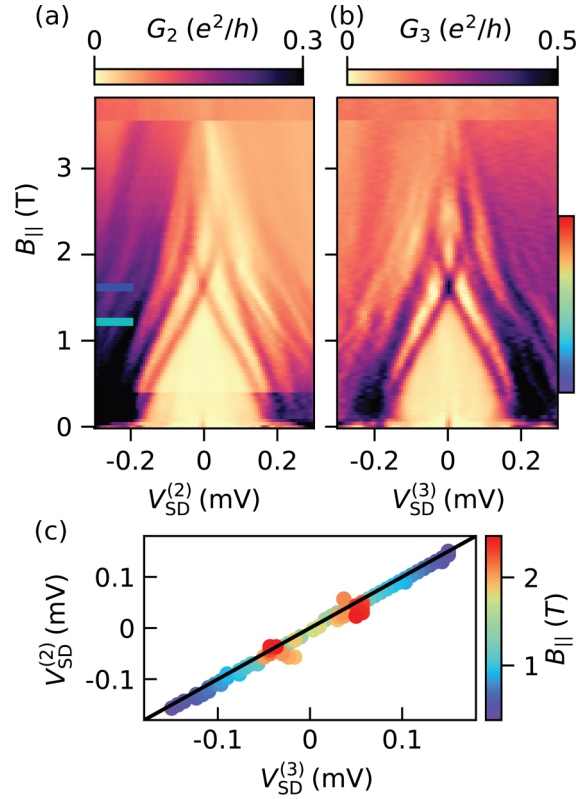

FIG. 3. (a) and (b) Tunneling spectroscopy with respect to magnetic field at the two ends of the nanowire (NW) with $V_{W23} = -3.09\,\mathrm{V}$ [marked with ⋆ on Figs. 2(b) and 2(c)]. Both measurements show subgap states crossing zero bias at $B_{||} = 1.6\,\mathrm{T}$ with a clear overshoot around $B_{||} = 2\,\mathrm{T}$. (c) Parametric plot of the extracted peak positions from the lowest energy subgap states in (a) and (b). The color of the points indicates the field value in accordance with the rainbow color bar in (b).

the ABSs at $B_{||} = 1.6\,\mathrm{T}$ followed by an overshoot at $B_{||} = 2\,\mathrm{T}$. The states appear in both tunneling conductance measurements of G_2 and G_3. We extracted the peak position in $V_{SD}^{2(3)}$ of the ABS from the measurements of G_2 and G_3. The parametric plot of the peak positions $V_{SD}^{(2/3)}$ of the ABSs in G_2 and G_3 in Fig. 3(c) shows that all points lie close to the identity line, suggesting strong correlations. Details about the extraction of the peak position are outlined in the Supplemental Material [44].

The ABSs seen in G_2 and G_3 evolve similarly with gate voltage V_{W23} and magnetic field $B_{||}$, suggesting that they belong to the same extended quantum states. Similar experimental findings have been made previously [45,46]. The magnetic field dependence of the states is furthermore characteristic for ABSs in short NWs [27].

Special points in the measurement in Fig. 2(b) are the crossing points of the horizontal resonances with the sharp vertical resonances. At these points, an ABS in the NW is on resonance with the QD in the tunnel barrier under the gate P_2. Tunneling spectroscopy G_2 using tunnel probe 2 at a field value of $B_{||} = 1.1\,\mathrm{T}$ while sweeping V_{P2} along the values given by the blue dashed line in Fig. 2(b) is shown in Fig. 4(a). The ABSs at $V_{SD}^{(2)} = \pm 0.05\,\mathrm{mV}$ were unaffected by the change of V_{P2} outside the range -0.040 to $-0.020\,\mathrm{V}$. Within this range, the QD resonance appears as a conductance enhancement at high bias, reflecting the fact that G_2 was being measured through the QD in tunnel barrier 2. As the QD went on resonance with the ABSs, the ABSs with lowest energy merged at zero bias before returning to their previous energies. This resulted in a characteristic bowtie shape of the resonances of the ABSs. A simultaneous measurement of G_3 during the sweep of V_{P2} at the other end of the NW is shown in Fig. 4(b). The enhancement of conductance at high bias due to the QD that was present in the measurement of G_2 was absent in the measurement of G_3. The ABSs, however, showed the same bowtie shape around the voltage value $V_{P2} \approx -0.030\,\mathrm{V}$ which corresponds to the resonance condition between the ABSs and the QD in tunnel barrier 2. Note that, in the measurement of both G_2 and G_3, not only the lowest energy ABSs undergo a change at the resonance condition with the QD but also the higher excited ABSs at $V_{SD}^{(2,3)} = \pm 0.12$ and $= \pm 0.20\,\mathrm{mV}$. In addition to the change in ABS energy, a clear change in the conductance peak height is visible when going through the resonance condition.

Around $B_{||} = 1.6\,\mathrm{T}$, the low-energy ABSs merged to yield a single conductance peak at zero bias. A measurement of G_2 with respect to V_{P2} in Fig. 4(c) shows that this peak was unperturbed except for voltage values around $V_{P2} \approx -0.030\,\mathrm{V}$, where the QD was on resonance with the ABSs. At this point, the QD led to a pair of arc-shaped resonances with strong conductance at $V_{SD}^{(2)} \approx \pm 0.05\,\mathrm{mV}$. Around the same value of gate voltage, the ABS resonances split symmetrically away from

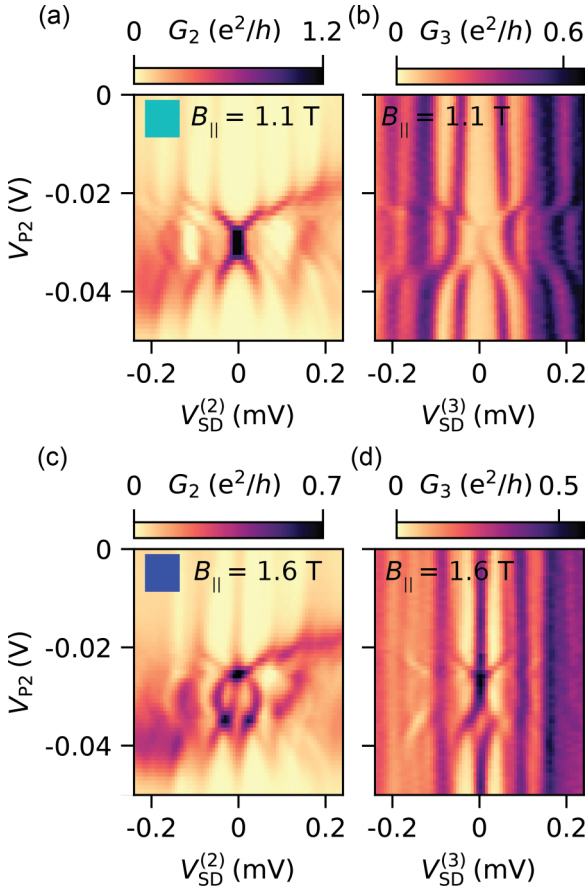

FIG. 4. (a) Tunneling conductance G_2 at the left side of the nanowire (NW) segment at $V_{W23} = -3.09$ V [marked with ⋆ and blue dashed line on Figs. 2(b) and 2(c)] as a function of the gate voltage V_{P2} which tunes the tunnel barrier. A quantum dot (QD) resonance is visible as an enhancement of conductance at high bias around $V_2 \approx -0.030$ V. The subgap states change their energy at the point of the QD resonance, drawing a characteristic bowtie shape. (b) Tunneling spectroscopy G_3 at the other end of the NW. The Andreev bound states (ABSs) show the same change in energy as visible in the measurement of G_2 in (a). (c) and (d) Same as (a) and (b) at higher parallel magnetic field, $B_{||}$. The ABSs split to form a diamond-shaped energy profile at the position of the QD resonance.

zero bias with a kink at $V_{SD}^{(2)} = \pm 0.03$ mV, forming a diamond shape. The simultaneous measurement of G_3 in Fig. 4(d) reveals similar V_{P2} dependence of the ABS energy. Note that the next excited states were located at $V_{SD}^{(2,3)} = \pm 0.09$ mV and were also affected around $V_{P2} \approx -0.030$ V, leading to a bowtie shape.

The appearance of ABSs with bowtie- and diamond-shaped patterns while on resonance with the QD level is an indication of the QD being sufficiently tunnel coupled to the ABSs such that the two energy levels significantly hybridize, consistent with theoretical and previous experimental results [36–39,47]. The measurement of the energy shift at both ends of the 0.6 μm NW, while a local gate voltage at only one end is changed, is a nonlococal signature of the delocalized ABSs. If tunneling spectroscopy is measured at both ends of a NW, hybridization of bound states with a local QD can be used as a quantum mechanical tool to test whether a quantum state extends through the whole NW, like the analysis of cross-conductance and correlated appearance at both ends [45,48]. This is in contrast to experiments where spectroscopy is performed at one end of a NW. In such a case, a QD in the absence of a bound states in the NW can mimic signatures of extended states inside the NW in tunneling spectroscopy [47,49–53].

In comparison with previous experiments, the present setup offers additional information about the spatial extent of the bound state, as one can perform tunneling spectroscopy at both ends of the NW segment. This also allows for the observation of the change in energy of the ABS at one position while it is being hybridized with a QD 0.6 μm away by means of changing a local gate. This nonlocal signature is a demonstration of the ABS being an extended quantum state. Note that we do not observe anticrossings of the bound state with the QD resonances in bias spectroscopy, which is consistent with the states being attributed to ABSs as opposed to partially overlapping Majorana zero modes [37].

In the Supplemental Material [44], we present data of the hybridization of an ABS in the NW segment under the gate labeled W_{12} with a local QD in the tunnel barrier. Results from a second device (device 2) are also presented. Device 2 is a slightly different design, with side probes that do not have Al leads, only the bare semiconductor. Device 2 showed similar results as device 1 when an ABS in a NW was brought onto resonance with a QD localized at one probe while observing the impact of the hybridization on the bound state at the other probe.

We thank Samuel Escribano, Karsten Flensberg, Max Geier, Andrea Maiani, Elsa Prada, Pablo San-Jose, and Waldemar Svejstrup for valuable discussions on theory and Abhishek Banerjee, Lucas Casparis, Asbjørn Drachmann, Esteban Martinez, Felix Passmann, Daniel Sanchez, Saulius Vaitiekėnas, and Alexander Whiticar for input on experimental aspects. We acknowledge support from the Danish National Research Foundation and a grant (Project No. 43951) from VILLUM FONDEN.

[1] P. Krogstrup, N. L. B. Ziino, W. Chang, S. M. Albrecht, M. H. Madsen, E. Johnson, J. Nygård, C. M. Marcus, and T. S. Jespersen, Nat. Mater. **14**, 400 (2015).

[2] Y. Liu, S. Vaitiekėnas, S. Martí-Sánchez, C. Koch, S. Hart, Z. Cui, T. Kanne, S. A. Khan, R. Tanta, S. Upadhyay *et al.*, Nano Lett. **20**, 456 (2020).

[3] F. Krizek, J. E. Sestoft, P. Aseev, S. Marti-Sanchez, S. Vaitiekėnas, L. Casparis, S. A. Khan, Y. Liu, T. Stankevič, A. M. Whiticar *et al.*, Phys. Rev. Mater. **2**, 093401 (2018).

[4] V. M. Pereira, C.-N. Wu, K. Höfer, A. Choa, C.-A. Knight, J. Swanson, C. Becker, A. C. Komarek, A. D. Rata, S. Rößler *et al.*, Phys. Status Solidi B **258**, 2000346 (2021).

[5] L. Fu and C. L. Kane, Phys. Rev. Lett. **100**, 096407 (2008).
[6] L. Fu and C. L. Kane, Phys. Rev. B **79**, 161408(R) (2009).
[7] X.-L. Qi, T. L. Hughes, and S.-C. Zhang, Phys. Rev. B **82**, 184516 (2010).
[8] R. S. K. Mong, D. J. Clarke, J. Alicea, N. H. Lindner, P. Fendley, C. Nayak, Y. Oreg, A. Stern, E. Berg, K. Shtengel *et al.*, Phys. Rev. X **4**, 011036 (2014).
[9] O. Lesser, G. Shavit, and Y. Oreg, Phys. Rev. Res. **2**, 023254 (2020).
[10] J. D. Sau, R. M. Lutchyn, S. Tewari, and S. Das Sarma, Phys. Rev. Lett. **104**, 040502 (2010).
[11] A. Cook and M. Franz, Phys. Rev. B **84**, 201105(R) (2011).
[12] R. M. Lutchyn, E. P. A. M. Bakkers, L. P. Kouwenhoven, P. Krogstrup, C. M. Marcus, and Y. Oreg, Nat. Rev. Mater. **3**, 52 (2018).
[13] D. J. Carrad, M. Bjergfelt, T. Kanne, M. Aagesen, F. Krizek, E. M. Fiordaliso, E. Johnson, J. Nygård, and T. S. Jespersen, Adv. Mater. **32**, 1908411 (2020).
[14] J. O. Yuan, K. S. Wickramasinghe, W. M. Strickland, M. C. Dartiailh, K. Sardashti, M. Hatefipour, and J. Shabani, J. Vac. Sci. Technol. A **39**, 033407 (2021).
[15] J. Shabani, M. Kjaergaard, H. J. Suominen, Y. Kim, F. Nichele, K. Pakrouski, T. Stankevic, R. M. Lutchyn, P. Krogstrup, R. Feidenhans'l *et al.*, Phys. Rev. B **93**, 155402 (2016).
[16] H. J. Suominen, M. Kjaergaard, A. R. Hamilton, J. Shabani, C. J. Palmstrøm, C. M. Marcus, and F. Nichele, Phys. Rev. Lett. **119**, 176805 (2017).
[17] M. Kjaergaard, H. J. Suominen, M. P. Nowak, A. R. Akhmerov, J. Shabani, C. J. Palmstrøm, F. Nichele, and C. M. Marcus, Phys. Rev. Appl. **7**, 034029 (2017).
[18] A. M. Whiticar, A. Fornieri, A. Banerjee, A. C. C. Drachmann, S. Gronin, G. C. Gardner, T. Lindemann, M. J. Manfra, and C. M. Marcus, Phys. Rev. B **103**, 245308 (2021).
[19] E. C. T. O'Farrell, A. C. C. Drachmann, M. Hell, A. Fornieri, A. M. Whiticar, E. B. Hansen, S. Gronin, G. C. Gardner, C. Thomas, M. J. Manfra *et al.*, Phys. Rev. Lett. **121**, 256803 (2018).
[20] F. Nichele, A. C. C. Drachmann, A. M. Whiticar, E. C. T. O'Farrell, H. J. Suominen, A. Fornieri, T. Wang, G. C. Gardner, C. Thomas, A. T. Hatke *et al.*, Phys. Rev. Lett. **119**, 136803 (2017).
[21] A. M. Whiticar, A. Fornieri, E. C. O'Farrell, A. C. Drachmann, T. Wang, C. Thomas, S. Gronin, R. Kallaher, G. C. Gardner, M. J. Manfra *et al.*, Nat. Commun. **11**, 3212 (2020).
[22] W. Chang, V. E. Manucharyan, T. S. Jespersen, J. Nygård, and C. M. Marcus, Phys. Rev. Lett. **110**, 217005 (2013).
[23] A. Jellinggaard, K. Grove-Rasmussen, M. H. Madsen, and J. Nygård, Phys. Rev. B **94**, 064520 (2016).
[24] E. J. H. Lee, X. Jiang, R. Žitko, R. Aguado, C. M. Lieber, and S. De Franceschi, Phys. Rev. B **95**, 180502(R) (2017).
[25] J.-D. Pillet, C. H. L. Quay, P. Morfin, C. Bena, A. L. Yeyati, and P. Joyez, Nat. Phys. **6**, 965 (2010).
[26] F. Nichele, E. Portolés, A. Fornieri, A. M. Whiticar, A. C. C. Drachmann, S. Gronin, T. Wang, G. C. Gardner, C. Thomas, A. T. Hatke *et al.*, Phys. Rev. Lett. **124**, 226801 (2020).
[27] Y. Huang, H. Pan, C.-X. Liu, J. D. Sau, T. D. Stanescu, and S. Das Sarma, Phys. Rev. B **98**, 144511 (2018).
[28] L. Hofstetter, S. Csonka, J. Nygård, and C. Schönenberger, Nature (London) **461**, 960 (2009).
[29] L. G. Herrmann, F. Portier, P. Roche, A. L. Yeyati, T. Kontos, and C. Strunk, Phys. Rev. Lett. **104**, 026801 (2010).
[30] M. Leijnse and K. Flensberg, Phys. Rev. B **84**, 140501(R) (2011).
[31] K. Gharavi, D. Hoving, and J. Baugh, Phys. Rev. B **94**, 155417 (2016).
[32] S. Hoffman, C. Schrade, J. Klinovaja, and D. Loss, Phys. Rev. B **94**, 045316 (2016).
[33] K. Flensberg, Phys. Rev. Lett. **106**, 090503 (2011).
[34] M. Leijnse and K. Flensberg, Phys. Rev. Lett. **107**, 210502 (2011).
[35] S. Plugge, A. Rasmussen, R. Egger, and K. Flensberg, New J. Phys. **19**, 012001 (2017).
[36] D. J. Clarke, Phys. Rev. B **96**, 201109(R) (2017).
[37] E. Prada, R. Aguado, and P. San-Jose, Phys. Rev. B **96**, 085418 (2017).
[38] M.-T. Deng, S. Vaitiekėnas, E. Prada, P. San-Jose, J. Nygård, P. Krogstrup, R. Aguado, and C. M. Marcus, Phys. Rev. B **98**, 085125 (2018).
[39] F. Peñaranda, R. Aguado, P. San-Jose, and E. Prada, Phys. Rev. B **98**, 235406 (2018).
[40] T. Zienkiewicz, J. Barański, G. Górski, and T. Domański, J. Phys.: Condens. Matter **32**, 025302 (2020).
[41] A. Ptok, A. Kobiałka, and T. Domański, Phys. Rev. B **96**, 195430 (2017).
[42] T. D. Stanescu and S. Das Sarma, Phys. Rev. B **97**, 045410 (2018).
[43] A. Grivnin, E. Bor, M. Heiblum, Y. Oreg, and H. Shtrikman, Nat. Commun. **10**, 1940 (2019).
[44] See Supplemental Material at http://link.aps.org/supplemental/10.1103/PhysRevB.106.L161301 for additional details of the materials, growth, and experiments, and additional data.
[45] G. L. R. Anselmetti, E. A. Martinez, G. C. Ménard, D. Puglia, F. K. Malinowski, J. S. Lee, S. Choi, M. Pendharkar, C. J. Palmstrøm, C. M. Marcus *et al.*, Phys. Rev. B **100**, 205412 (2019).
[46] P. Yu, J. Chen, M. Gomanko, G. Badawy, E. P. A. M. Bakkers, K. Zuo, V. Mourik, and S. M. Frolov, Nat. Phys. **17**, 482 (2021).
[47] A. Vuik, B. Nijholt, A. Akhmerov, and M. Wimmer, SciPost Phys. **7**, 061 (2019).
[48] G. C. Ménard, G. L. R. Anselmetti, E. A. Martinez, D. Puglia, F. K. Malinowski, J. S. Lee, S. Choi, M. Pendharkar, C. J. Palmstrøm, K. Flensberg *et al.*, Phys. Rev. Lett. **124**, 036802 (2020).
[49] C.-X. Liu, J. D. Sau, T. D. Stanescu, and S. Das Sarma, Phys. Rev. B **96**, 075161 (2017).
[50] E. J. H. Lee, X. Jiang, M. Houzet, R. Aguado, C. M. Lieber, and S. De Franceschi, Nat. Nanotechnol. **9**, 79 (2014).
[51] M. Valentini, F. Peñaranda, A. Hofmann, M. Brauns, R. Hauschild, P. Krogstrup, P. San-Jose, E. Prada, R. Aguado, and G. Katsaros, Science **373**, 82 (2021).
[52] C.-X. Liu, J. D. Sau, and S. Das Sarma, Phys. Rev. B **97**, 214502 (2018).
[53] H. Pan and S. Das Sarma, Phys. Rev. Res. **2**, 013377 (2020).